Available online at www.sciencedirect.com
ScienceDirect
Materials Research Bulletin 42 (2007) 696–706
Materials Research Bulletin
www.elsevier.com/locate/matresbu

Synthesis, characterization and photocatalytic properties of nanosized Bi_2WO_6, $PbWO_4$ and $ZnWO_4$ catalysts

Hongbo Fu, Chengsi Pan, Liwu Zhang, Yongfa Zhu *

Department of Chemistry, Tsinghua University, Beijing 100084, PR China

Received 22 April 2006; received in revised form 19 June 2006; accepted 25 July 2006
Available online 30 August 2006

Abstract

Nanosized Bi_2WO_6, $PbWO_4$ and $ZnWO_4$ photocatalysts were synthesized by a mild hydrothermal crystallization process. The physical and photophysical properties of the catalysts were characterized by X-ray diffractometry, Brunauer–Emmet–Teller surface area and porosity measurements, transmission electron microscopy, Raman spectra, and diffused reflectance spectroscopy. The rhodamine-B photodegradation in aqueous medium was employed as a probe reaction to test the photoactivities of the as-prepared samples under four irradiation wavelengths. Bi_2WO_6 not only presented the photocatalytic activity in the wide spectral scope, including UV and visible light but also exhibited the strong photosensitized capability to transform RhB under visible light irradiation ($\lambda > 490$ nm). $ZnWO_4$ only displayed relatively high photoactivity under UV irradiation. However, $PbWO_4$ showed poor photoactivity under any light irradiation. On the basis of the calculated density functional theory (DFT), the photocatalytic mechanisms were discussed.

Keywords: A. Oxides; B. Chemical synthesis; C. Raman spectroscopy; D. Catalytic properties; D. Semiconductivity

1. Introduction

Semiconductor photocatalysis has been the focus of many investigations because of its application for the destruction of chemical contaminants and water splitting [1–4]. Over the recent decade, a variety of mixed metal oxides have also been extensively studied as a new class of photocatalysts [5–13]. The representative catalysts with potential activities for overall water splitting include $SrTiO_3$ [5], $NaTaO_3$ [6], ZrO_2 [7], $K_4Nb_6O_{17}$ [8], and Ta_2O_5 [9]. Among the catalysts examined to date, $NaTaO_3$ doped with La has demonstrated the highest quantum yield of water splitting, exceeding 50% when irradiated by UV light. A few examples have also been applied to environmental treatment of organic pollutants, such as $CaIn_2O_4$ [11], $CaBi_2O_4$ [12], and $BiVO_4$ [13]. Zou et al. [12] reported that $CaBi_2O_4$ showed the high visible-light-induced photoactivities for the decomposition of both acetaldehyde and methylene blue.

Recently, Kudo and Hijii found that Bi_2WO_6 has a suitable valence band for photocatalytic O_2 evolution from water under visible light irradiation [14]. More recently, Zou et al. reported that Bi_2WO_6 show not only the activity for photocatalytic O_2 evolution but also the activity of mineralizing both $CHCl_3$ and CH_3CHO contaminants under visible light irradiation [15]. They pointed out that the high photoactivity of Bi_2WO_6 could be attributed to the WO_6 layered

* Corresponding author. Tel.: +86 10 6278 7601; fax: +86 10 6278 7601.
E-mail addresses: zhuyf@mail.tsinghua.edu.cn, Zhuyf@chem.tsinghua.edu.cn (Y. Zhu).

0025-5408/$ – see front matter © 2006 Elsevier Ltd. All rights reserved.
doi:10.1016/j.materresbull.2006.07.017

structure, which was beneficial to the transfer of electrons to the surface of the photocatalyst along the layered network because the recombination between photoinduced electrons and holes was depressed by the electron transfer to a layered host [14,15].

The other tungstate materials, such as $PbWO_4$ and $ZnWO_4$, have strong application potential in various fields, including photoluminescence, microwave applications, optical fibers, scintillator materials, humidity sensors, magnetic properties, and catalysis [16]. It has been found they hold unique combination of physical and chemical properties, in terms of molecular and electronic versatility, reactivity, and stability [17–19]. Therefore, $PbWO_4$ and $ZnWO_4$, similarly to Bi_2WO_6, could be the candidates for potential photocatalysts.

These compounds were conventionally prepared by high temperature solid-state calcinations [14,15]. Recently, environmentally friendly aqueous processes have received much attention. This is the process in which materials are synthesized under mild conditions in nonharmful solvents such as water. Apparently, suitable synthetic approaches may give raise to particular properties due to possible variation of surface morphology and structure. The hydrothermal synthesis offers many advantages over conventional solid-state methods, such as mild synthesis conditions, high degree of crystallinity, high purity and narrow particle size distribution of product [20–22]. More importantly, much higher efficiency of the photocatalyst synthesized by this method could be expected from the specific nanostructure of the product. The present authors have already reported [23] that Bi_2WO_6 nanosheet prepared by a simple hydrothermal process showed higher photocatalytic activity for the degradation of the pollutants compared to the one prepared by the solid-state calcinations.

In the present work, nanosized Bi_2WO_6, $ZnWO_4$ and $PbWO_4$ catalysts were firstly prepared by the hydrothermal synthesis. On the basis of the surface characterization, the photocatalytic activities of the catalysts for decomposition of the pollutants were evaluated, and the photocatalytic mechanism of the catalysts were also discussed. As far as we know, the photoactivities of tungstate were seldom reported. Especially, $PbWO_4$ was observed as a photocatalyst for the first time to degrade the pollutants.

2. Experimental

2.1. Catalysts preparation

The catalysts were prepared by the hydrothermal synthesis [17–19]. The details are as follows—(1) Bi_2WO_6: 0.485 g $Bi(NO_3)_3{\cdot}5H_2O$, 0.125 H_2WO_4 and 0.28 g KOH were added to 9 mL deionized water with magnetic stirring; (2) $ZnWO_4$: 0.001 mol $Na_2WO_4{\cdot}2H_2O$ and 0.001 mol $Zn(NO_3)_2$ were added to 9 mL deionized water with magnetic stirring to form a homogeneous solution. The solution pH was adjusted to 11 by using 0.5 M NaOH or HCl; (3) $PbWO_4$: 1.656 g $Pb(NO_3)_2$, 1.247 g H_2WO_4 were added to 9 mL deionized water with magnetic stirring. The solution pH was adjusted to 11 by using 0.5 M KOH or HNO_3.

The reaction mixtures were sealed in a Teflon-lined stainless steel autoclave and heated at 180 °C under autogenous pressure for 24 h. After cooling, the product was filtered, washed and dried at ambient temperature. All chemicals were reagent grade quality and were used without further purification. TiO_2 P-25 (mainly in the anatase form, surface area is 50 $m^2\ g^{-1}$) was obtained from Degussa (Germany). All aqueous solutions were made up in deionized and doubly distilled water.

2.2. Sample characterization

Powder X-ray diffraction (XRD) of Cu Kα radiation was measured using a Bruker D8 Advance X-ray diffractometer and a 2θ scan rate of $2^\circ\ min^{-1}$. Transmission electron microscopy (TEM) images of the samples were obtained in a JEOL JEM-1200EX operated at 120 kV. The samples were prepared by dispersing the powders in water and depositing a drop of suspension onto a thin Formavar film supported on a Cu grid. The specific surface area (S_{BET}) was calculated by the Brunauer–Emmet–Teller (BET) method on the basis of nitrogen uptake measured at −196 °C. Porosity was monitored from the nitrogen adsorption–desorption isotherms obtained at the liquid nitrogen temperature with a Sorptomatic 1900 Carlo Erba Instrument. UV–vis diffuse reflectance spectra (DRS) of the samples were measured with a Hitachi U-3010 spectrometer. $BaSO_4$ was the reference sample and the spectra were recorded in the range 200–700 nm. Raman spectra were measured under a microscope using a 50× objective to focus the incident excitation laser radiation into a spot 1–2 μm diameter, and to collect the scattered light. The spectra were obtained

using a Renishaw RM2000 spectrometer equipped with notch filter and a CCD detector. The atomic rations of the so-prepared samples were measured using X-ray fluorescence (XRF-1700, Shimadzu).

2.3. Photochemical experiments

The RhB photodegradation was tested as a model reaction to evaluate the photocatalytic activities of the catalysts. The photocatalytic experiments were performed under four irradiation wavelength, namely $\lambda = 254$ nm, $\lambda > 290$ nm, $\lambda > 420$ nm and $\lambda > 490$ nm. The irradiation light ($\lambda = 254$ nm) was obtained by a 12 W Hg lamp (Institute of Electric Light Source, Beijing) and the average light intensity was 50 μW cm^{-2}. In the case of the other irradiation lights, a 500 W xenon lamp ($\lambda > 290$ nm, Institute of Electric Light Source, Beijing) was focused through a window, and a 420 or 490 nm cutoff filter was placed onto the window face of the cell to ensure the desired irradiation light. The average light intensities were 40 and 30 mW cm^{-2}, respectively. The irradiation light ($\lambda > 290$ nm) was acquired by using the full wavelength of the xenon lamp, and no additional filter was employed. The average light intensity was 50 mW cm^{-2}. The radiant flux was measured with a power meter from the Institute of Electric Light Sources (Beijing, China).

The photocatalytic reaction was carried out with 0.05 g of powdered photocatalysts suspended 100 mL of RhB solution in a glass cell. The mixture was sonicated before illumination and stored in the dark for a further 30 min to obtain the saturated absorption of RhB onto the catalysts. The pH of the solution was not adjusted and the solution is central (pH 7.5). After UV or visible light illumination, 3 mL aliquots were taken out at regular time intervals. The catalyst was removed from solution by a centrifuger at 4000 rpm, and the supernatant was used for the quantitative analysis of the pollutants. The change in the concentration in each degraded solution was monitored on a Hitachi U-3010 spectrometer by measuring the absorbance in 553 nm for RhB. The deionized water was used as the reference sample.

2.4. DFT electronic structure calculations

The quantum-mechanical calculations performed here are based on density functional theory (DFT) [24]. Exchange-correlation effects were taken into account using the generalized gradient approximation (GGA) [25]. The total energy code CASTEP was used, which utilizes pseudopotentials to describe electron–ion interactions and represents electronic wavefunctions using a plane-wave basis set [26].

3. Results and discussion

3.1. Characterization of the as-prepared samples

The morphologies and microstructures of the as-prepared samples were firstly investigated with TEM. Three marked morphologically different crystallites, rod-like particles for $PbWO_4$, needle-like ones for $ZnWO_4$ and sheet-like ones for Bi_2WO_6, are shown in Fig. 1A–C, respectively. All images were appeared to be high crystallinity. $PbWO_4$ particles were inhomogeneous and the crystallite sizes were in the range from several tens to several hundreds nanometer. Yielded particles for $ZnWO_4$ were typically acicular and consist of several domains along the needle (α-) axis, and these single crystals were measured between 0.5 and 1.2 μm in length. Bi_2WO_6 crystals displayed mainly thin sheet-shaped morphology with borders of a few of hundreds nanometer. The samples hold large primary sheets and smaller secondary ones. The close-folded agglomerations of the irregular sheets were clearly presented.

The surface textural properties of the as-prepared samples were assessed by nitrogen adsorption measurements at -196 °C, and the nitrogen adsorption isotherms and pore size distributions are shown in Fig. 2. The pore size distribution of $ZnWO_4$ sample was narrowest (<55 nm), suggesting that the crystals were most monodisperse, compared to Bi_2WO_6 and $PbWO_4$. The wide distribution of the pore sizes (~142 nm) confirmed that $PbWO_4$ crystals were dispersed widely. Bi_2WO_6, $ZnWO_4$ and $PbWO_4$ presented their largest fraction of pore diameter in the region of 17, 50 and 28 nm, respectively. Bi_2WO_6 and $ZnWO_4$ exhibited relatively high surface areas with respect to the ones synthesized by the solid-state reaction method [23]. The surface area of 46.4 m^2 g^{-1} for Bi_2WO_6 and 36.7 m^2 g^{-1} for $ZnWO_4$ was gained, respectively. However, there was an exception for $PbWO_4$ sample. The significant low surface area of 2.34 m^2 g^{-1} was available. The low surface area of $PbWO_4$ prepared by the hydrothermal method was reported by Hu and Zhu [27].

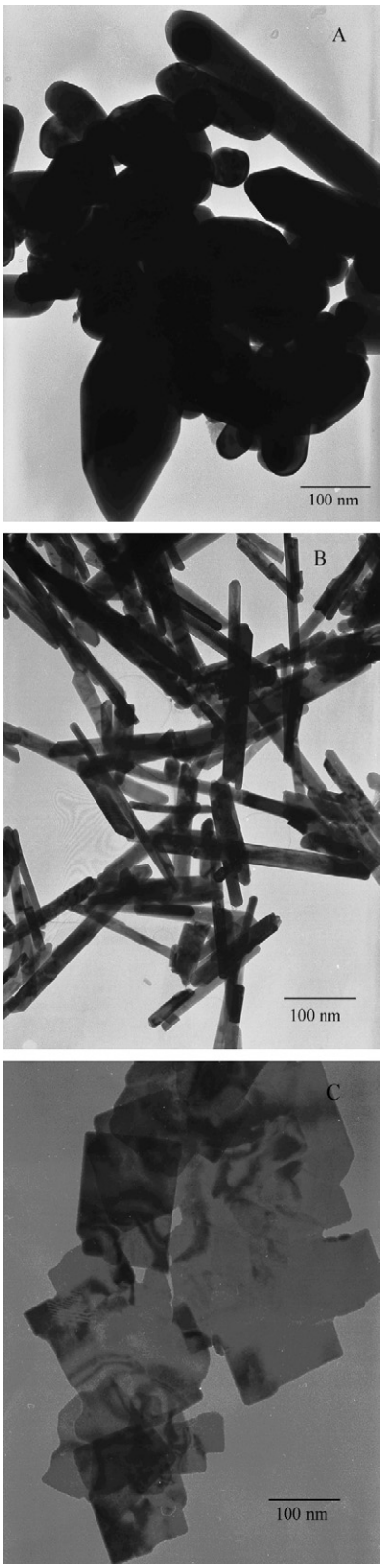

Fig. 1. TEM images of $PbWO_4$ (A), $ZnWO_4$ (B) and Bi_2WO_6 (C) catalysts prepared by the hydrothermal synthesis under the different conditions.

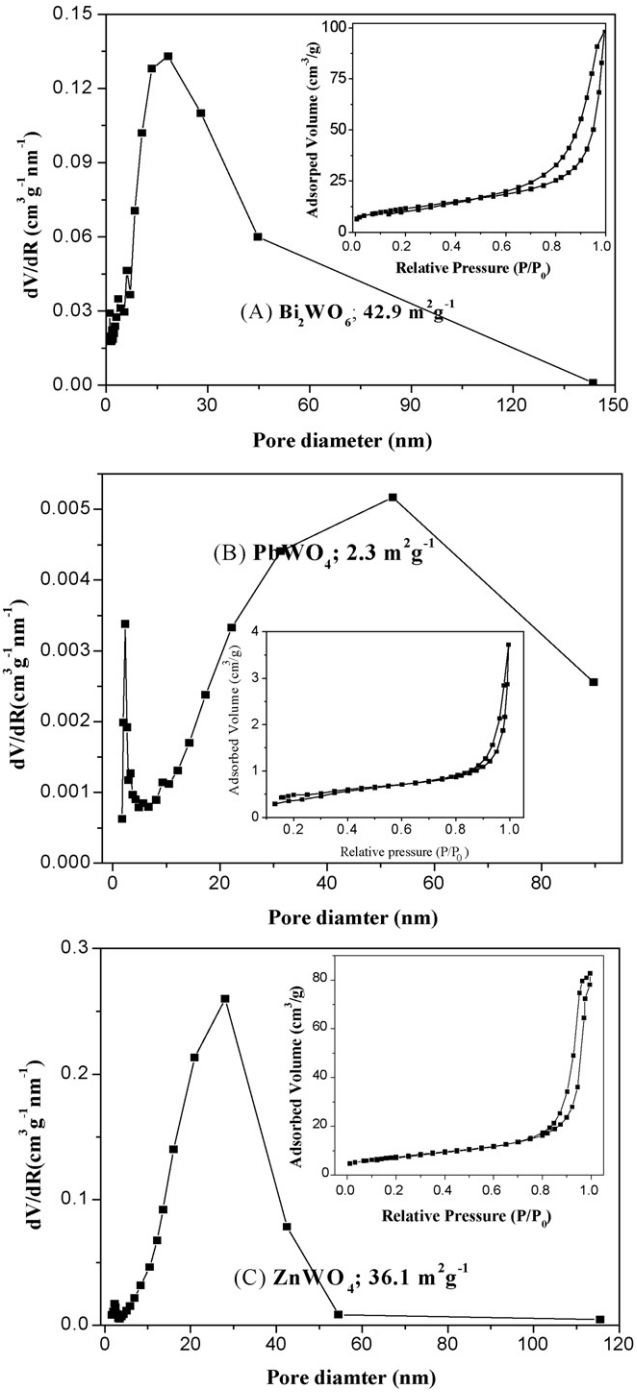

Fig. 2. N_2 adsorption–desorption isotherms (inset) and Barret–Joyner–Halenda (BJH) pore size distribution plots of Bi_2WO_6, $PbWO_4$ and $ZnWO_4$ catalysts.

XRD patterns of the as-prepared samples were found to be identical with the expected oxides on the basis of the literatures (Bi_2WO_6: JCPDS 73-1126; $ZnWO_4$: JCPDS 73-0554; $PbWO_4$: JCPDS 85-1857) [17–19], as shown in Fig. 3. The rounding of the baseline spectra indicated the presence of trace amounts of amorphous oxides. XRD patterns of the samples revealed sharp and symmetric peaks, indicating the high crystallinity of the crystals. The single phases of the tetragonal, monoclinic and orthorhombic structure were available for $PbWO_4$, $ZnWO_4$ and Bi_2WO_6,

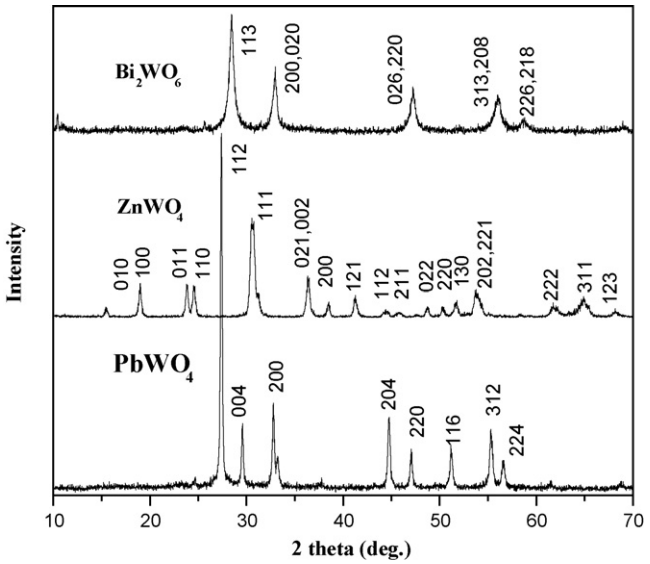

Fig. 3. XRD patterns of Bi_2WO_6, $PbWO_4$, and $ZnWO_4$ catalysts, prepared by the hydrothermal synthesis at the different conditions.

respectively. Any impurity could not be found from XRD patterns. The parameters of the crystal structures of $PbWO_4$, $ZnWO_4$ and Bi_2WO_6 are shown in Table 1. $PbWO_4$, $ZnWO_4$ and Bi_2WO_6 belong to tetragonal, monoclinic and orthorhombic system, respectively. Their structure are notable different. $ZnWO_4$ and $PbWO_4$ possess WO_4 tetrahedron, but Bi_2WO_6 hold WO_6 octahedron structure. Therefore, their photocatalytic performance could be markedly different.

Raman spectra of the samples are shown in Fig. 4. On the basis of the previous publications [28], the peaks in the range 600–1000 cm^{-1} were assigned to the stretches of the W–O bands. In more detail, the bands at 790 and 820 cm^{-1} of Bi_2WO_6 were associated with the antisymmetric and symmetric A_g modes of terminal O–W–O. The band of 310 cm^{-1} could be assigned to translational modes involving simultaneous motions Bi^{3+} and WO_4. In the case of $PbWO_4$, the band around 900 cm^{-1} represented the strain activated $v_1(B_u)$ infrared band. The two v_2 modes were observed at 319 cm^{-1} (A_g) and 351 cm^{-1} (B_g). As for $ZnWO_4$, the striking band about 900 cm^{-1} was interpreted as an antisymmetric bridging mode associated with the tungstate chain. The bands about 300 cm^{-1} were assigned to the modes of terminal WO_2 group. The W–O bonds of intermediate length (about unit valency) are characteristic of bridging W–O bonds and are assigned to Raman mode stretching wavenumbers in the 700–1000 cm^{-1}. A higher Raman stretching mode wavenmuber indicates a more distorted structure, whereas a lower Raman stretching mode wavenmuber indicates a more regular structure [30]. $ZnWO_4$ and $PbWO_4$ present a strong peak at 800 cm^{-1}, and Bi_2WO_6 shows two-peaks at 910 cm^{-1}, suggesting that Bi_2WO_6 holds a more distorted structure and the W–O bond of the WO_6 octahedron is shorter than one of the WO_4 octahedron in $ZnWO_4$ and $PbWO_4$ catalysts [29].

It is difficult to detect impurities presence from LRS, because the stretches of the impurity, such as Bi_2O_3, ZnO and PbO were likely to overlap with one of the tungstates. Quantitative results give the atomic ration of 1:1.05, 1:1.05 and 1:1.08 for Bi_2O_3/WO_3, ZnO/WO_3 and PbO/WO_3. It was close to the ideal value considering the instrumental error. Therefore, the impurity such as Bi_2O_3, ZnO and PbO, could be not available when the catalysts were prepared by the mild hydrothermal process.

The photoabsorption abilities of these samples were detected by UV–vis DRS. The spectra are shown in Fig. 5. Bi_2WO_6 reveal the strongest absorbance between 200 and 370 nm. Nevertheless, the considerable absorption band in the visible region was expected to be responsible for the photodegradation of the pollutants under visible light

Table 1
Parameters of the crystal structures of Bi_2WO_6, $PbWO_4$ and $ZnWO_4$

$PbWO_4$ (system: tetragonal; space group: $I41/a$)	a: 5.4619, α: 90.0; b: 5.4619, β: 90.0; c: 12.049; γ: 90.0
$ZnWO_4$ (system: monoclinic; space group: $P2/c$)	a: 4.6910, α: 90.0; b: 5.7200, β: 90.6; c: 4.9250; γ: 90.0
Bi_2WO_6 (system: orthorhombic; space group: $Pca2_1$)	a: 0.5437, α: 90.0; b: 1.6430, β: 90.0; c: 0.5458, γ: 90.0

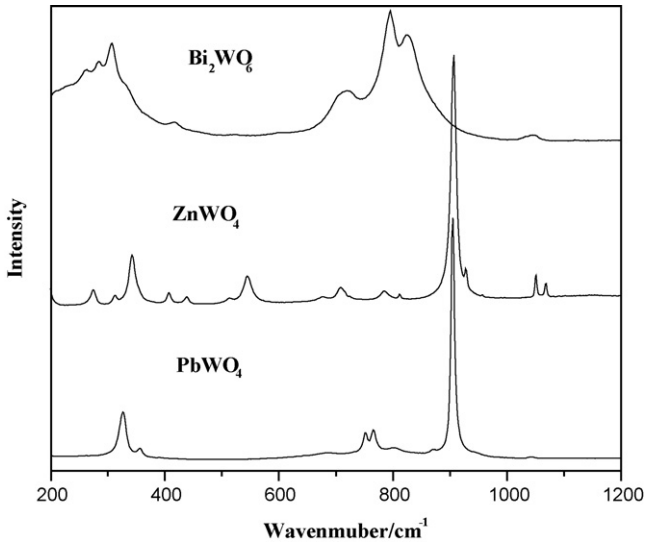

Fig. 4. Raman spectra of Bi_2WO_6, $PbWO_4$, and $ZnWO_4$ catalysts, prepared by the hydrothermal synthesis at the different conditions.

irradiation. $PbWO_4$ also presented the photoabsorption properties from UV region to visible region shorter than 520 nm. The steep shape of the spectra indicated that the visible light absorption is not due to the transition from the impurity level but is due to the band-gap transition. $ZnWO_4$ exhibited photoabsorption properties only in the UV region shorter than 400 nm. The color of $PbWO_4$, $ZnWO_4$ and Bi_2WO_6 were yellow, pale and pale-yellow, respectively, as predicted from their UV–vis spectra, which were correlated with their band structure. The band wide (determined by the linear extrapolation of the steep part of UV–vis light absorption toward the baseline) was 2.70 eV for Bi_2WO_6, 2.43 eV for $PbWO_4$ and 3.31 eV for $ZnWO_4$ from their absorbance band [15,30].

3.2. Photocatalytic activities of the catalysts

The photodegradation of RhB was firstly tested as a model reaction to evaluate the photocatalytic activity of the catalysts. By comparison, the photodegradation of RhB in the presence of P-25 was also performed. The results are shown in Fig. 6. UV light (λ = 254 nm) could alone promote the photodegradation of RhB. Twenty percent of RhB was direct transformed by UV light. All catalysts displayed the photoactivity. P-25 presented the highest photoactivity to

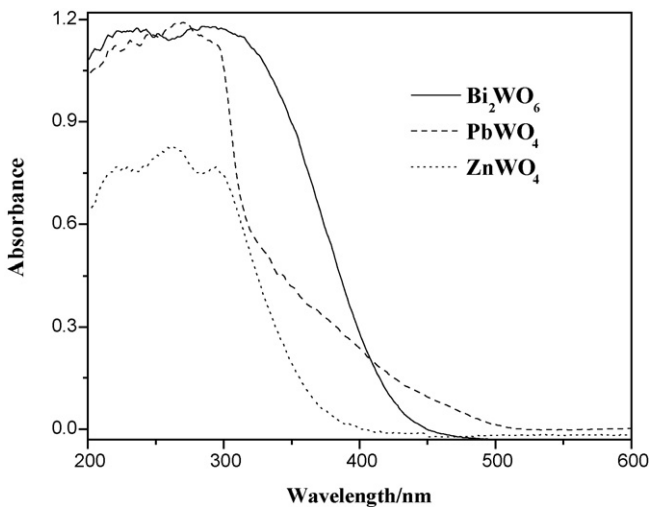

Fig. 5. UV–vis DRS of Bi_2WO_6, $PbWO_4$, and $ZnWO_4$ catalysts, prepared by the hydrothermal synthesis at the different conditions.

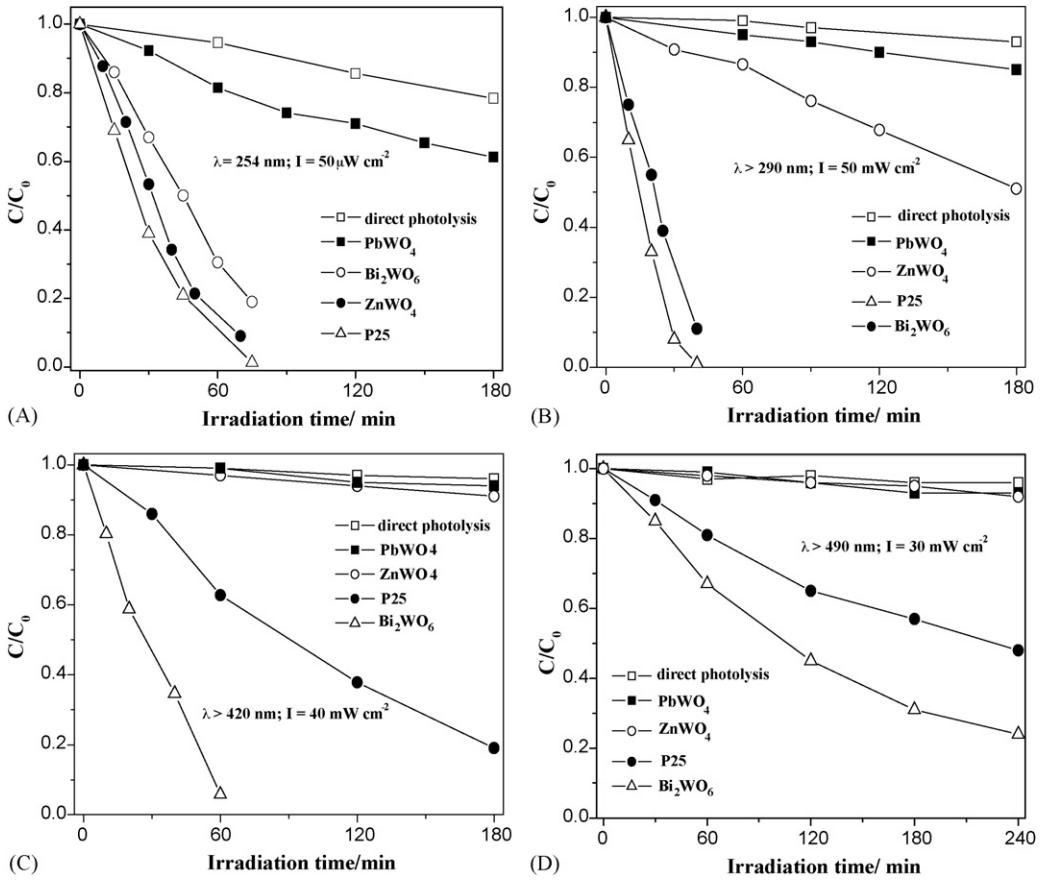

Fig. 6. Photocatalytic photodegradation of RhB (1×10^{-5} M L^{-1}) in the different suspensions (catalyst loading, 0.5 g L^{-1}) under different irradiation wavelength.

transform RhB. $PbWO_4$ showed the weak capability to transform RhB. When irradiated for 180 min, 40% of RhB is degraded by $PbWO_4$. However, $ZnWO_4$ and Bi_2WO_6 exhibited comparatively high photocatalytic activity. Almost completely degradation of RhB was acquired after 90 min. The catalysts showed activity in the followed order: P-25 > $ZnWO_4$ > Bi_2WO_6 > $PbWO_4$. In the case of the light ($\lambda > 290$ nm), all catalysts were still photocatalytically active for the degradation of RhB. In the presence of Bi_2WO_6, completely degradation of RhB was gained after 60 min irradiation. Fifty percent of RhB was transformed by $ZnWO_4$ after 180 min. $PbWO_4$ presented the weakest photoactivity for the degradation of RhB. Only 10% of RhB could be degraded when the experiment were performed for 180 min. The activity of the catalysts are in the order of P-25 > Bi_2WO_6 > $ZnWO_4$ > $PbWO_4$. In the case of $\lambda > 420$ nm and $\lambda > 490$ nm, Bi_2WO_6 presented higher capability to photocatalytic RhB, compared to P-25. Whereas, $PbWO_4$ and $ZnWO_4$ were not active for the degradation of RhB under such conditions. These results indicated that Bi_2WO_6 hold an excellent photocatalytic performance in the wide light region. $ZnWO_4$ was only active in the UV region. $PbWO_4$ displayed poor photoactivity for the degradation of RhB under any irradiation light.

Bi_2WO_6 also showed the activity when the light wavelength was much longer than 490 nm, where it absorbed poorly the light radiation. It is well known that RhB can absorb visible light in the range 400–600 nm, which is attributed to the ground state and the excited state of the dye. Therefore, it is postulated that the RhB photodegradation was attributed to the photocatalysis of Bi_2WO_6 assisted by RhB dye absorbed on the Bi_2WO_6 surface. This process might be similar to the surface sensitization of TiO_2 via adsorbed dyes [31]. When $\lambda > 490$ nm, RhB is only the light absorbing species. From the dye-excited state, an electron is injected into the CB of Bi_2WO_6 where it is captured by the surface adsorbed O_2 to produce $O_2^{\bullet -}$, and the dye cation radicals are decomposed subsequently via attack by oxygen active species. When irradiated by the light ($\lambda > 490$ nm), $PbWO_4$ and $ZnWO_4$ did not present the photosensitized capability to degrade RhB, which could be due to their different crystal structure [17–19].

In our previous work [32], the photodegradation of 4-CP by Bi_2WO_6 has been performed. It was founded that Bi_2WO_6 was active for the photodegradation of 4-CP, suggesting that Bi_2WO_6 is indeed active under visible-light irradiation. We choose 4-chlorophenyl (4-CP) as an additional pollutant to study the photoactivities of $ZnWO_4$ and $PbWO_4$ under visible-light irradiation ($\lambda > 420$ nm). They show the poor activity for the photodegradation of 4-CP (not shown).

Bi_2WO_6 and $ZnWO_4$ catalysts as a kind of heterogeneous photocatalyst can be easily recycled by a simple filtration because their large density. After the photodegradation of RhB, the catalysts were filtrated and characterized by XRD. XRD analysis of the samples showed that the crystal structures of the photocatalysts were not changed after the photocatalytic reaction, confirming both Bi_2WO_6 and $ZnWO_4$ catalysts were stable during the photocatalytic reaction. The stability of a photocatalyst is important to its application; doped TiO_2 photocatalysts sometimes suffer from this problem [31]. However, the pH of the solution exerts a notable effect on the stability of such catalysts. Bi_2WO_6 is unstable in the acidic solution, which has been reported in our previous work [32]. $ZnWO_4$ present a similar speciality.

3.3. Calculated band structures of the catalysts

The energy level and the band gap of the oxide semiconductor will play a crucial role in determining photocatalytic activity. The electronic structure of Bi_2WO_6 and $ZnWO_4$ have been investigated by plane wave density functional theory (DFT) calculations in our previous reports [32,33]. The DOS calculations indicates that the valence bands of $ZnWO_4$ consist of the occupied O 2p orbitals, whereas the bottom of the conduction bands is composed of the empty W 5d orbitals [33]. As for Bi_2WO_6, the valence band of the catalyst consists of O 2p + Bi 6p hybrid orbitals. The bottom of conduction band was formed by the W 5d orbitals, with a small contribution of the Bi 6p. Thus, the highest occupied and lowest unoccupied molecular orbital levels were composed of the hybrid orbitals of the O 2p and Bi 6s 6p orbitals and the W 5d orbitals, respectively [32].

Fig. 7 shows the energy band dispersion diagram and DOS for $PbWO_4$. The DOS showed four occupied bands and an unoccupied band. The lowest band consisted of the Pb 5d + O 2s hybrid orbitals (1–18#). The second and third bands were made up of the Pb 6s (19–20#) and the O 2p + W 5d hybrid orbitals (21–32#), respectively. The fourth bands, i.e., the valence bands were composed of the O 2p orbital. The bottom of conduction band was formed by the W 5d + Pb 6p hybrid orbitals (45–56#), with a small contribution of the O 2p. Thus, the highest occupied and lowest unoccupied molecular orbital levels were composed of the O 2p and the hybrid of the Pb 6p orbitals and the W 5d orbitals, respectively.

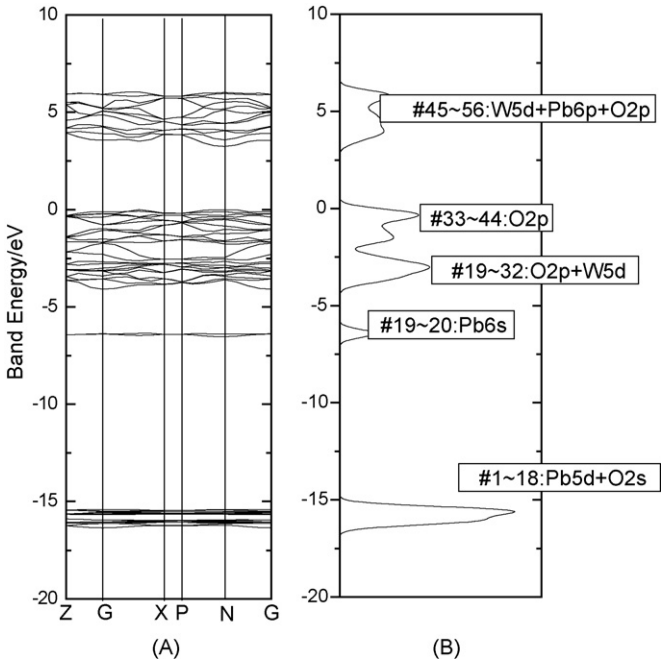

Fig. 7. DFT calculations for $PbWO_4$: (A) energy band dispersion; (B) density of states.

3.4. Mechanism of photocatalytic property of the catalysts

On the basis of the results of DFT calculations [32,33], UV absorption of $ZnWO_4$ could be due to the charge-transfer transition between tungsten and oxygen in WO_4^{2-}. In the case of Bi_2WO_6, the transition of the 6s electrons of Bi^{3+} to the empty 5d orbital of W^{5+} becomes possible. Such a transition has been also observed in the $BiNbO_4$ [34], $BiTaO_4$ [35] and $BiVO_4$ [36]. This transition due to the 6s electrons usually occurs at a lower energy than the charge-transfer transition in WO_6^{6-}. Therefore, the valence bands may be formed by not only Bi 6s but also O 2p, namely a hybrid orbitals of Bi 6s and O 2p. $PbWO_4$, similarly to Bi_2WO_6, the visible light absorption was due to the transition from a valence band formed by Pb 5s or a hybrid orbital of Pb 5s and O 2p to a conduction band of W 5d. Therefore, from DRS spectra (Fig. 5) one can see that the absorbance of Bi_2WO_6 show an apparent red shift compared to one of $ZnWO_4$.

It was interesting to note that $PbWO_4$ showed photoabsorption in the visible light region ($\lambda < 520$ nm). This means that the photocatalysts have the ability to respond to wavelengths in the visible light region. However, this photocatalyst did not work under visible light irradiation ($\lambda > 400$ nm) in our experiment. Furthermore, it exhibited the poor activity even under UV irradiation as compared to $ZnWO_4$ and Bi_2WO_6. Although direct absorption of photons by the band gap of oxides can generate electron–hole pairs, there could exist the fast recombination of electron–hole pairs, resulting that the e^- and h^+ could not migrate to the surface to react with the adsorbed reactants. However, as for Bi_2WO_6, the hybridization of the Bi 6s and O 2p levels makes the VB largely dispersed, which favors the mobility of photoholes in the VB and is beneficial to the oxidation reaction. From LRS spectra, Bi_2WO_6 show a higher Raman stretching mode wavenmuber (910 cm^{-1}) compared to the ones (800 cm^{-1}) of $ZnWO_4$ and $PbWO_4$, which indicates a more distorted structure. The high photoactivity of Bi_2WO_6 could also be attributed to this distorted WO_6 layered structure, which was beneficial to the transfer of electrons to the surface of the photocatalyst along the layered network because the recombination between photoinduced electrons and holes was depressed by the electron transfer to a layered host.

4. Conclusions

Nanosized Bi_2WO_6, $PbWO_4$, $ZnWO_4$ catalysts were synthesized by the mild hydrothermal crystallization. The photocatalytic experiments revealed that $ZnWO_4$ was relatively active to phototransform RhB under UV irradiation ($\lambda = 254$ nm). Bi_2WO_6 not only showed the capability to degrade RhB under UV irradiation, but also could efficiently photodegrade RhB under visible irradiation. $PbWO_4$ presented the poor activity to photodegrade RhB even under the UV irradiation.

Our work suggests that the idea of using Bi_2WO_6 and $ZnWO_4$ could be a plausible strategy to develop an efficient photocatalyst for the destruction of pollutants. The further investigation on the photochemical properties of the tungstates is under a way and is expected to be a communication in the future.

Acknowledgments

The authors appreciate Chinese National Science Foundation (20433010), Trans-Century Training Program Foundation for the Talents by the Ministry of Education, P. R. C. and the Excellent Young Teacher Program of MOE, P. R. China for financial support.

References

[1] M.R. Hoffmann, S.T. Martin, W. Choi, Chem. Rev. 95 (1995) 69.
[2] M.A. Fox, M.T. Dulay, Chem. Rev. 93 (1993) 341.
[3] C.C. Wong, W. Chu, Environ. Sci. Technol. 37 (2003) 2310.
[4] W. Ho, J. Yu, J. Lin, P. Li, Langmuir 20 (2004) 5865.
[5] K. Domen, A. Kudo, T. Onishi, J. Catal. 10 (1986) 217.
[6] H. Kato, A. Kudo, Catal. Lett. 295 (1998) 487.
[7] K. Sayama, H. Arakawa, J. Phys. Chem. 97 (1993) 531.
[8] A. Kudo, K. Sayama, A. Tanaka, K. Asakura, K. Domen, K. Maruya, T. Onishi, J. Catal. 120 (1989) 337.
[9] K. Sayama, H. Arakawa, J. Photochem. Photobiol. A: Chem. 77 (1994) 243.

[10] Q. Zhang, L. Gao, Langmuir 20 (2004) 9821.
[11] J. Tang, Z. Zou, J. Ye, Chem. Mater. 16 (2002) 1644.
[12] J. Tang, Z. Zou, J. Ye, Angew. Chem. Int. Ed. 43 (2004) 4463.
[13] S. Kohtani, M. Koshiko, A. Kudo, K. Tokumura, Y. Ishigaki, A. Toriba, K. Hayakawa, R. Nakagaki, Appl. Catal. B: Environ. 46 (2003) 573.
[14] A. Kudo, S. Hijii, Chem. Lett. (1999) 1103.
[15] J. Tang, Z. Zou, J. Ye, Catal. Lett. 92 (2004) 53.
[16] S. Seong, K.-A. Yee, T.A. Albright, J. Am. Chem. Soc. 115 (1993) 1981.
[17] V. Nagirnyi, M. Kirm, A. Kotlov, A. Lushchik, L. Jonsson, J. Luminesc. 102 (2003) 597.
[18] S. Yu, B. Liu, M. Mo, J. Huang, X. Liu, Y. Qian, Adv. Funct. Mater. 13 (2003) 639.
[19] Y. Shi, S. Feng, C. Cao, Mater. Lett. 44 (2000) 215.
[20] M. Andersson, L. Osterlund, S. Ljungstrom, A. Palmqvist, J. Phys. Chem. B 106 (2002) 10674.
[21] B. Liu, S. Yu, L. Li, F. Zhang, Q. Zhang, M. Yoshimura, P. Shen, J. Phys. Chem. B 108 (2004) 2788.
[22] J.G. Yu, J.F. Xiong, B. Cheng, Y. Yu, J.B. Wang, J. Solid State Chem. 178 (2005) 1968.
[23] C. Zhang, Y. Zhu, J. Phys. Chem. B 109 (2004) 22432.
[24] W. Kohn, L.J. Sham, Phys. Rev. A 140 (1965) 1133.
[25] J.P. Perdew, Y. Wang, Phys. Rev. B 45 (1992) 13244.
[26] M.C. Payne, M.P. Teter, D.C. Allan, T.A. Arias, J.D. Joannopoulos, Rev. Mod. Phys. 64 (1992) 1045.
[27] X. Hu, Y. Zhu, Langmuir 20 (2004) 1521.
[28] M. Crane, R. Forst, P. Williams, T. Kloprogge, J. Raman Spectrosc. 33 (2002) 62.
[29] F. Hardcastle, I. Wachs, J. Raman Spectrosc. 26 (1995) 397.
[30] M.A. Butler, Appl. Phys. 48 (1977) 1914.
[31] T. Wu, G. Liu, J. Zhao, J. Phys. Chem. B 103 (1999) 4862.
[32] H. Fu, C. Pan, W. Yao, Y. Zhu, J. Phys. Chem. B 109 (2005) 22432.
[33] H. Fu, J. Lin, L. Zhang, Y. Zhu, Appl. Catal. A 306 (2006) 58.
[34] M. Wiegel, W. Middel, G. Blasse, J. Mater. Chem. 5 (1995) 981.
[35] S. Tokunaga, H. Kato, A. Kudo, Chem. Mater. 13 (2001) 4624.
[36] A. Kudo, K. Omore, H. Kato, J. Am. Chem. Soc. 121 (1999) 11459.